Journal of Environmental Chemical Engineering 11 (2023) 109977

Contents lists available at ScienceDirect

Journal of Environmental Chemical Engineering

journal homepage: www.elsevier.com/locate/jece

The importance of superoxide anion for *Escherichia coli* biofilm removal using plasma-activated water

Binbin Xia [a], Heema Kumari Nilesh Vyas [a,b], Renwu Zhou [a,c,*], Tianqi Zhang [a], Jungmi Hong [a], Joanna G. Rothwell [d], Scott A. Rice [e], Dee Carter [b,d], Kostya (Ken) Ostrikov [f], Patrick J. Cullen [a], Anne Mai-Prochnow [a,**]

[a] School of Chemical and Biomolecular Engineering, The University of Sydney, Australia
[b] Sydney Institute for Infectious Diseases, The University of Sydney, Australia
[c] State Key Laboratory of Electrical Insulation and Power Equipment, Center for Plasma Biomedicine, Xi'an Jiaotong University, Xi'an, China
[d] School of Life and Environmental Sciences, The University of Sydney, Australia
[e] Agriculture and Food, Microbiomes for One Systems Health, Commonwealth Scientific and Industrial Research Organisation, Sydney, Australia
[f] School of Chemistry and Physics and QUT Centre for Biomedical Technologies, Queensland University of Technology, Brisbane, QLD 4000, Australia

ARTICLE INFO

Editor: Xin Yang

Keywords:
Plasma activated water
Bubble spark discharge reactor
Biofilm
Escherichia coli
Reactive species
Superoxide anion radicals

ABSTRACT

Microbial biofilms cause contaminations in different environmental settings, including pipelines, filters, membranes, food and processing infrastructure. They ultimately pose a major risk to human health and necessitate costly cleaning and repair. Cold plasma, a partially ionised gas, and plasma-activated water (PAW) exhibit powerful disinfectant activity. However, the optimal generating conditions, such as the choice of gas used to produce PAW, remain unclear. Here, a range of different PAWs were generated from argon, nitrogen, air, and oxygen in a plasma bubble spark discharge (BSD) reactor capable of directly treating *Escherichia coli* (ATCC 25922) biofilms in situ. We measured the reactive oxygen and nitrogen species (RONS) (H_2O_2, NO_3^-, NO_2^-) in PAW and the excited species via optical emission spectroscopy (OES). PAW generated using oxygen (PAW-O_2) was the most effective and completely removed *E. coli* biofilms on stainless steel surfaces. Confocal microscopy demonstrated that PAW treatment removed most biofilm cells from the surface with only a few dead cells remaining. We demonstrated that intracellular ROS level increases significantly in the PAW-O_2-treated biofilms. Using molecular scavengers, we showed that superoxide anion radical ($\bullet O_2^-$) played a critical role in the inactivation of *E. coli* biofilms. We also confirmed the generation of $\bullet O_2^-$ in the PAW-O_2 via electron paramagnetic resonance (EPR) spectrometry. The potential chemical reactions that occurred in PAW were hypothesized via optical emission spectra (OES). Our results demonstrate the importance of input gas and plasma operating conditions to maximise effective RONS production for optimal biofilm removal under real environmental and industry-relevant conditions.

1. Introduction

Contamination of surfaces in contact with biofilm-forming bacteria is a major problem for drinking water supplies, industrial water processing systems, membranes, filters, and food processing stainless-steel units [8,30,56]. Biofilms are particularly hard to eradicate because of their higher resistance to antimicrobials and disinfectants compared to planktonic cells [4,6]. Such contamination can lead to equipment failure, energy losses, product contamination, and environmental pollution, resulting in adverse human health outcomes and significant costs to industries [3]. Therefore, a new decontamination method is critically needed that can effectively decontaminate resistant biofilms, whilst also avoiding damage to the surface of the treated material or leaving toxic chemical residues.

One promising treatment method with these characteristics is cold atmospheric plasma (CAP) processing. Plasma is the fourth state of matter and is generated when a gas is exposed to an electric field voltage, leading to the ionisation of gas molecules and the generation of

* Corresponding author at: School of Chemical and Biomolecular Engineering, The University of Sydney, Australia.
** Corresponding author.
E-mail addresses: renwu.zhou@xjtu.edu.cn (R. Zhou), anne.mai-prochnow@sydney.edu.au (A. Mai-Prochnow).

https://doi.org/10.1016/j.jece.2023.109977
Received 24 January 2023; Received in revised form 5 April 2023; Accepted 19 April 2023
Available online 22 April 2023

diverse excited and reactive species [36]. CAP presents a broad range of antimicrobial activity, including antibacterial, antiviral, and antifungal actions [5,13,23,44,62]. The antimicrobial activity is mainly attributed to the formation of reactive oxygen and nitrogen species (RONS) [5,15,54,65]. RONS encompasses both transient species, such as hydroxyl radical (OH), atomic oxygen (O), peroxynitrite anion (ONOO-), and superoxide anion (O_2), which have been shown to have a half-life of just a few seconds, or even less than one second, as well as more stable species like ozone (O_3), hydrogen peroxide (H_2O_2), and nitrogen oxides (NO_x), which can persist for several minutes, days, or even years [67].

An innovative way of using CAP as an antimicrobial technology is to generate the plasma discharge in water to produce plasma-activated water (PAW) [36]. PAW has the potential to be used as a washing step and is suitable for large-scale applications in chemical engineering industries [29]. It is appropriate for disinfecting sensitive and hard-to-access surfaces, including food and heat-sensitive devices [33,40].

While plasma is generally effective, the optimal generating conditions and mode of action are still unclear. Diverse PAW production methods have been explored, including plasma discharge above the water surface, plasma discharges in bubbles dissolved in the water, and direct plasma discharges in the water [11,24,67]. The design and operating conditions significantly affect the plasma composition [1,37,54,58,67]. Not surprisingly, the use of different operating gases leads to the generation of different cocktails of active species, which determine the antimicrobial efficacy [41,64]. While CAP can be generated using a range of gases or gas mixtures, different gases lead to the formation of unique combinations of reactive species. Air, argon, nitrogen and oxygen are frequently used as working gases [7,27,38,51,57], and in particular, the addition of oxygen leads to the generation of ROS with strong antibacterial effects [64].

An important aspect when generating PAW is the electrode design. Most PAW studies to date typically use a plasma discharge that is generated close to the water surface [18,28,32]. Such a design can limit the penetration of the plasma species that are formed in the gas phase into the water. On the other hand, our previous research demonstrated that an underwater plasma discharge-generated PAW provided a higher antimicrobial reactivity compared to conventional plasma jet reactors [46]. The current study utilises a submerged PAW system called a bubble spark discharge (BSD) [45] which allows a much larger surface area for reactive species to diffuse into the water via plasma gas bubbles in a system (Fig. 1). This BSD system has previously shown to exhibit acute antimicrobial activity against planktonic bacteria in situ using air as the discharge gas [45]. Other underwater plasma discharge electrodes have also been shown to have antimicrobial activity against planktonic bacteria cells [33,41].

While most of the research studies have investigated the antimicrobial efficacy of PAW against planktonic bacteria, the bacteria biofilm state that survives on surfaces thrives the real threat to several industries. Therefore, it is critical to test the antimicrobial efficacy of PAW against biofilms. In the present study, *E. coli* biofilms grown on stainless-steel surfaces were chosen to study the disinfectant efficacy of the PAW generated with different gas sources (argon, nitrogen, oxygen, and atmospheric air). We found that the physical and chemical properties and the resulting antimicrobial efficacy of the generated PAW vary depending on the chosen gas source. Therefore, in this study, our focus was to identify the chemical species formed in the PAW generated via the differing gas inputs and study their pH, oxidation-reduction potential (ORP), and electrical conductivity (EC). Then *E. coli* biofilms treated with the PAW were investigated for their viability (colony forming units, live/dead staining coupled with confocal microscopy), and intracellular biofilm ROS accumulation.

2. Materials and methods

2.1. Strain and biofilm formation

Escherichia coli ATCC 25922 was routinely maintained on tryptic soy agar (TSA) (tryptone (pancreatic digest of casein) 17.0 g/L, soytone (peptic digest of soybean) 3.0 g/L, glucose 2.5 g/L, sodium chloride 5.0 g/L, dipotassium phosphate 2.5 g/L, agar 15 g/L). One colony from a fresh agar plate was inoculated into 10 mL tryptic soy broth TSB) and

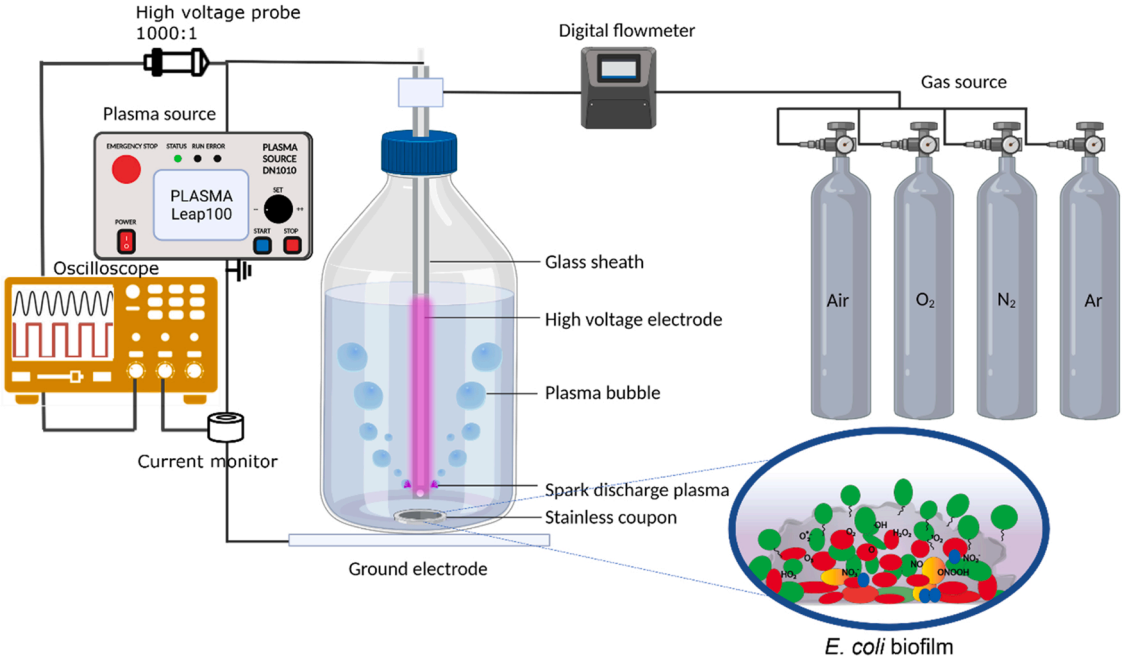

Fig. 1. A schematic illustration of the in-situ biofilm treatment using plasma-activated water (PAW) generated by a bubble spark discharge (BSD) plasma reactor. An *E. coli* biofilm was grown on a stainless-steel coupon and placed at the bottom of the Schott bottle containing 100 mL of MilliQ water. The plasma bubble reactor consists of a high-voltage electrode and a glass sheath. To generate spark discharge plasma, the high-voltage electrode was powered by PlasmaLeap100. The voltage and current of the power source are monitored by the oscilloscope equipped with a high-voltage probe and a current monitor.

incubated for 14 h at 37 °C, shaking at 160 rpm. For biofilm formation, the overnight cultures were diluted 1/100 to obtain an approximate cell density of 10E5 CFU/mL. 1 mL of the diluted culture was inoculated into wells of a 24-well plate containing sterile stainless-steel coupons (diameter: 12.7 mm and thickness: 3.8 mm from BioSurface Technologies, Bozeman, Montana, USA). Plates were incubated for 48 h at 30 °C with 110 rpm shaking to allow for cell attachment and subsequent biofilm formation.

2.2. Plasma treatment

The plasma bubble reactor (PlasmaLeap Technologies, Sydney) consists of a metal rod high voltage electrode inside a quartz tube (Fig. 1) with four holes (0.5 mm diameter each) evenly spaced at the immersed end to allow for the plasma discharge to contact the water. The gas flow was controlled by a digital M series mass flow meter (Alicat Scientific, United States). Coupons with the attached biofilm were aseptically removed from the well plate and placed into 250 mL Schott bottles containing 100 mL sterile MilliQ (Fig. 1). The plasma bubble reactor was submerged in the water containing the coupons for direct plasma chemical experiment [29].

The plasma-activated water (PAW) was generated as previously described [45]. Briefly, a Leap100 (PlasmaLeap Technologies, Sydney) power source was used with an input voltage of 150 V, a discharge frequency of 1500 Hz, a resonance frequency of 60 kHz and a duty cycle of 100 μs. The treatment time was 10 min with 1 standard liter per minute (slm) of gas flow. Four different gases were tested, including argon (Ar), nitrogen (N_2), air, and oxygen (O_2). As a control, coupons were placed into 100 mL sterile MilliQ for 10 min

2.3. Cell enumeration

Immediately following the PAW treatment, coupons were extracted from the treatment bottle and placed into a Falcon tube containing 2 mL 1x phosphate buffered saline (PBS). The biofilm was removed from the coupon surface by scraping it with a sterile flat-end spatula and placed into falcon tubes. The Falcon tubes were then submerged in a sonicating water bath for 3 min at 45 kHz followed by 10 s vortexing to ensure complete dislodgement of biofilms. This did not affect cell viability (data not shown). Serial dilutions were then drop-plated (10 μL) onto TSA in triplicates. Plates were incubated overnight at 37 °C before determining the colony-forming units (CFU).

2.4. PAW reactive species measurements

Concentrations of hydrogen peroxide (H_2O_2), nitrate (NO_3^-), and nitrite (NO_2^-) along with pH, temperature, and electrical conductivity were assessed in the PAW generated using argon, N_2, air, and O_2 gases for 10 min. The concentration of H_2O_2 was measured by a titanium sulphate method [66] where H_2O_2 reacts with titanium oxysulphate ($TiOSO_4$) resulting in a yellow-coloured complex (pertitanic acid) that is quantified with UV-Vis spectroscopy at 408 nm (the standard curve of H_2O_2 is shown in supportive information Fig. S1). NO_3^- and NO_2^- species were measured using a Hanna Instrument multiparameter photometer (HI83399) with colorimetric nitrate kit (HI93766–50) and colorimetric nitrite reagent (HI93708–0), respectively. All standards were prepared in MilliQ water. pH, temperature, electrical conductivity (EC), and oxidation-reduction potential (ORP) were measured using a Hanna Instrument pH/ISE/EC meter (HI5522) supplied with a double junction pH electrode (HI12300), temperature probe (HI7662-W), a four-ring conductivity probe (HI76312), and an OPR electrode (HI3131), respectively.

2.5. Optical emission spectroscopy

The optical emission spectra (OES) of the plasma discharges generated in nitrogen, air, argon, and oxygen at 150 V, 1500 Hz were obtained by a spectrometer (Andor Shamrock SR-500i optical emission spectrometer, Oxford Instruments, UK) referred to a recent published method [26].

2.6. Molecular scavenger experiments

To investigate the effect of specific active species that were generated in the plasma, a range of molecular scavengers were used as previously described [45], including 200 mM Mannitol (scavenges hydroxyl radical), 100 μm uric acid (scavenges ozone), 20 mM Tiron (scavenges superoxide anion), 100 mM N-Acetyl-L-cysteine (general antioxidant and free radical scavenger), and 10 mM Sodium pyruvate (scavenges hydrogen peroxide). The scavengers were added directly into the treatment bottle before the plasma generation commenced.

2.7. EPR measurement of superoxide anion radicals

The formations of superoxide and superoxide-related hydroxyl radicals were detected with an electron paramagnetic resonance (EPR) spectrometer (Bruker Elexys E580, Bruker Inc., Billerica, MA, USA) using a spin trap DMPO (5,5-dimethylpyrroline-N-oxide). Spectra were recorded at room temperature, with microwave power at 10 dB and a modulation amplitude of 2.0 Gauss. The scanning time was 60 s and repeated 5 times in all experiments. The PAW was activated in 100 mL of MilliQ water using 4-hole bubble spark dielectric plasma reactor with an oxygen flow rate of 1slm. After 60 s of activation, 125 μL of the PAW-O_2 was collected and was measured immediately by EPR after mixing with 11.5 μL of pure DMPO. The PAW-O_2 with 20 mM Tiron (PAW-O_2 + Tiron) and MilliQ water bubbled with O_2 gas (but no plasma) with the same amount of DMPO were used as the control.

2.8. Confocal microscopy

Live/dead staining was performed on the biofilms formed on the coupon surfaces (Syto9 for viable cells and propidium iodide for dead cells, Invitrogen) according to the manufacturers' instructions. Briefly, 10 μL of the staining solution was added directly to the coupons with the attached biofilms and incubated in the dark for 10 min. The coupons were then transferred to a microscopy dish with a glass coverslip bottom and examined using a Nikon Ti-E confocal microscope equipped with a 40x objective. The Excitation/Emission wavelengths (Ex/Em) for Syto9 and PI are 480/500 nm and 490/635 nm, respectively.

2.9. Detection of intracellular ROS

Biofilms were stained with 2',7'-dichlorofluorescin diacetate (DCFDA) to assess intracellular ROS according to the manufacturers' instructions. Briefly, a 96-well plate containing 48 h *E. coli* biofilms was washed once with 150 μL MilliQ and challenged for 30 min with control (MilliQ), PAW-O_2, and PAW-O_2 + Tiron scavenger. Biofilms were then stained with 150 μL of 20 μM DCFDA solution (or 150 μL MilliQ for background controls) and incubated in the dark for 30 min. Once stained, the excess stain was removed, and biofilms were washed once with 150 μL MilliQ. Fluorescence was detected via ClarioStar plate reader at an Ex/Em of 485–15 nm/535–15 nm.

2.10. Statistical analysis

Experiments were performed 3 times and values are expressed as mean ± standard deviation ($\mu \pm \sigma$). A parametric, unpaired t-Test (2 tail, $p < 0.05$) or a One-way ANOVA (with Tukeys multiple comparisons test, $p < 0.05$) was performed where appropriate to identify significant differences in log reduction of each sample compared to the control.

3. Results and discussion

3.1. Biofilm removal using different input gases for the generation of PAW

Biofilms grown on stainless steel coupons were placed into the Schott bottle during the 10 min PAW generation time and remaining viable cells were enumerated by CFU counting. A significant reduction in CFU was observed for the PAW generated with all of the 4 gases when compared to the control (Fig. 2), with a 2-log reduction for the PAW-air, 1 log for the PAW-N_2 and 0.5 log for the PAW-Ar. A complete reduction in viability was only seen for biofilms treated with PAW-O_2 (6-log reduction). To further characterize the kinetic inactivation of PAW on 48 h-grown *E. coli* biofilm, the D-value (Decimal value: exposure time to achieve 1-log reduction) was calculated. Our results show that PAW-O_2 exhibited the shortest D-value (1.72 min), followed by PAW-Air (5.29 min), PAW-N_2 (10.91 min), and PAW-Ar (15.56 min). Several other studies use a D-value to shed light on the inactivation kinetics of cold plasma mediated cell death [10,50]. Interestingly, the achieved D-values ranges considerably, depending on the initial bacterial concentration, attachment surface and plasma treatment conditions. A study by Sen and Mutlu [47] calculated the D-value of pure oxygen DBD plasma that can effectively inactivate *E. coli* grown on stainless steel surfaces. The most efficient result with the fastest kinetics had a larger D-value of 22.9 ± 3.3 min when powered by 100 Watt plasma compared to our study. Recent research by Fernández-Gómez et al., [9] achieved a D-value of 11.3 min for *L. monocytogenes* biofilms with a final comparable (5.6-log) reduction in a stainless steel exposed to PAW generated by a surface DBD cold plasma reactor for 30 min.

While several studies have found PAW to be strongly antibacterial for planktonic cells [42,49], the reduction of biofilm cells to undetectable levels is a rare finding. Here, after only a 10-min treatment, we have demonstrated the efficacy of our PAW, which is a very promising result given that biofilms are highly resistant to most antimicrobials and removal strategies. As summarised in Table 1, Pan et al.[39] achieved a comparable (6-log) reduction of *Enterococcus faecalis* biofilm in a dental unit waterline system treated by the PAW generated by 260 L/h of air plasma jet, however, this consumed around four times more gas than this study. The PAW generated by BSD reactor supplied with Argon exhibited biofilm removal activity on both gram-positive and gram-negative bacteria-formed biofilm, ranging from 2 to 3.6 log reduction [35]. Other studies report considerably more modest reductions in biofilms by PAW [53].

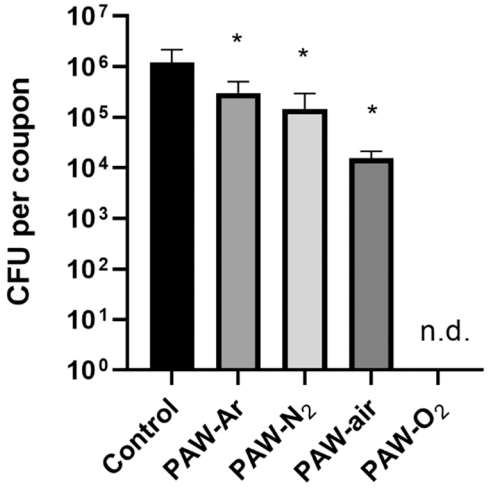

Fig. 2. Reduction of *E. coli* biofilms using PAW generated in argon, nitrogen, air, and oxygen assessed by CFU. 48 h biofilms were grown on stainless steel coupons and treated with PAW generated with different gases in a bubble reactor. All four treatment conditions were significantly different from the control, but only PAW-O_2 caused a complete loss of biofilm viability ($P < 0.05$, unpaired t-Test).

Table 1
Comparisons between the results of this study and other relevant research.

Reactor	PAW-supplied gas (input volume)	Biofilm bacteria strains	Reduction (log_{10})	Reference
BSD	Argon (3.1 L/min)	*Pseudomonas aeruginosa (PAO1) Pseudomonas libanensis Enterobacter cloacae*	3.3–3.6 log	Mai-Prochnow et al. [35]
BSD	Argon (3.1 L/min)	*Kocuria carniphila*	2 log	Mai-Prochnow et al. [35]
Plasma jet	Air (260 L/h)	*Enterococcus faecalis*	6 log	Pan et al. [39]
Plasma jet	Air (42.5 L/h)	*Enterobacter aerogenes*	3.0–3.8 log	Tan, Karwe [53]
BSD	O_2 (1 L/min)	*E. coli (ATCC25922)*	6.1 log	This study

The inactivation kinetics of *E. coli* biofilms when exposed to plasma are suggested to have a three phases mechanism, including the destruction of DNA by UV irradiation, erosion of the microorganism through intrinsic photo-desorption, and etching [47]. However, as the treatment has complex effects on cells, for example, gene regulation that affects the metabolism of starch and sucrose and thus carbohydrate transport and metabolism functions [9], determining the survival curve of bacterial biofilms that are exposed to plasma remains a challenging task.

3.2. Characterisation of PAW generated with different gases

We have demonstrated that the PAW-O_2 leads to the highest CFU reduction of *E. coli* biofilms, but the PAW generated with three other gases (Ar, N_2, and air) also showed antimicrobial activity. It is widely accepted that RONS produced in the PAW are responsible for their antibacterial effect [14,34,48]. The amount and type of RONS in the different PAW types will significantly affect antimicrobial activity. The formation of RONS in PAW is complex as there are many physical and chemical properties in play. In our plasma-generating experimental design, using a bubble spark discharge (BSD) electrode, a constant gas flow results in the plasma being bubbled through four small holes at the bottom of the glass cover for the electrode (Fig. 1). The gaseous plasma surrounding the electrode contains several reactive species. The contact of the plasma bubble with the water then leads to the generation of a large amount of short- and long-lived ROS and RNS, mainly including reactive oxygen atoms, anions and ions, including (O, O(^{1}D), $^1O_2$, O_2^+, and O_2^-), $^\bullet$OH, $ONOO^-$, NO, H_2O_2, NO_2^-, NO_3^-, O_3 [36]. Because the highest CFU reduction was observed when biofilms were treated with the PAW-O_2, we hypothesised a higher concentration of certain antimicrobial species are generated in the PAW-O_2 compared to the other PAWs. To characterise the physical and chemical properties of the four different PAW, types of ROS (H_2O_2), and RNS (NO_2^-, NO_3^-) as well as the pH, temperature, electronic conductivity, and ORP were determined.

H_2O_2 (a known antimicrobial RONS generated in PAW) was predominant in the PAW-Ar and the PAW-O_2 (Fig. 3A). Specifically, after 10 min plasma treatment, PAW-Ar showed the highest amount of H_2O_2 (54.94 ± 1.39mg/L) while the PAW-air showed the lowest amount of H_2O_2 (4.10 ± 0.19mg/L. The PAW-O_2 (15.09 ± 0.38mg/L) showed a similar amount of H_2O_2 compared to the PAW-N_2 (13.95 ± 0.24mg/L). A high ROS concentration such as H_2O_2 is often linked to the bactericidal efficacy of the PAW [12]. However, our CFU results indicate the highest antimicrobial activity for the PAW-O_2 and not the PAW-Ar that had the highest H_2O_2 levels, indicating that H_2O_2 is not the main reactive species responsible for biofilm removal in our study. Nevertheless, H_2O_2 may

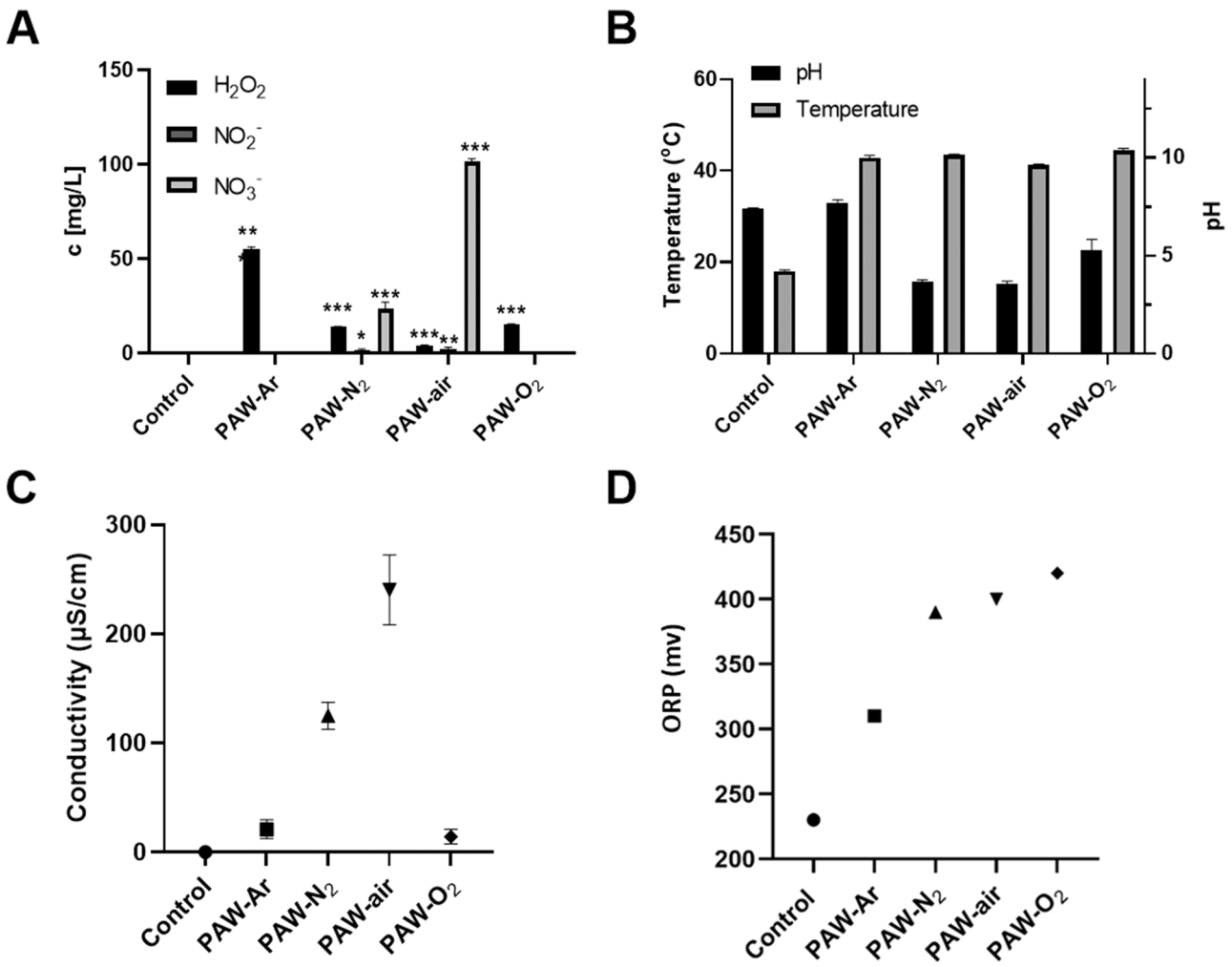

Fig. 3. Physical and chemical characterisation of PAW-Ar, PAW-N_2, PAW-air and PAW-O_2. A) reactive oxygen and nitrogen species of hydrogen peroxide (H_2O_2), (NO_3^-), and nitrite (NO_2^-), B) pH and temperature, C) electric conductivity, and D) oxidation-reduction potential (ORP) values of PAW using four different gas sources (argon, N_2, air, and O_2) at 10 min treatment time. Error bars represent standard deviation of three experiment repetitions.

still contribute to bacterial inactivation. In the acidic environment of the PAW, H_2O_2 concentration along with the O_2^- radical contributes mostly to the oxidation properties of the PAW [54]. However, in contrast to our results, it was found that the PAW (air) generated a higher amount of H_2O_2 compared to the PAW (nitrogen) [41]. The authors contributed this to the formation of more NOx species in air spark plasma leading to the consumption of H_2O_2 in the PAW (air) compared to the PAW (nitrogen).

High amounts of NO_3^- and NO_2^- were detected in the PAW-air (NO_3^-: 101.40 ± 1.56 mg/L; NO_2^-: 2.00 ± 1.00mg/L) and lower amounts in the PAW-N_2 (NO_3^-: 23.53 ± 3.49mg/L; NO_2^-:1.67 ± 0.58mg/L), (Fig. 3A), NO_3^- and NO_2^- were non-detectable in the PAW-Ar and the PAW-O_2. According to a previous study [41], NO_2^- in the PAW reacts with dissolved ozone and H_2O_2 to give NO_3^-, which makes NO_2^- less stable than NO_3^- in the PAW. At first, it seems unusual for the PAW-air to have a higher NO_3^- /NO_2^- content than the PAW-N_2. However, other authors reported a similar result where a 20% ratio of O_2/(O_2 +N_2) (-equivalent to air) gas composition generated more NO_3^- and NO_2^- than 100% N_2. One possible mechanism is that with the addition of O_2 in the gas, the atomic oxygen O emission can react with excited nitrogen species to form •NO, resulting in generation of more abundant NO_3^- and NO_2^- species [14].

PAW has been shown to have a low pH and this may further contribute to its antimicrobial activity [32,63]. The negative charge of some RNS (NO_3^- and NO_2^-) can lead to the acidification of the solution [46], which might catalyze the antibacterial activity of PAWs [5,15,65].

As shown in Fig. 3B, the lowest pH value was obtained when the PAW is generated using air (3.55 ± 0.16) with similarly low pH values ($p > 0.05$) for the PAW-N_2 (3.67 ± 0.09) and the PAW-O_2 (5.29 ± 0.54) In contrast the pH of the PAW-Ar (7.67 ± 0.02) remained similar to the control (7.41 ± 0.02) which is due to the lack of NO_x species [2]. A recent study of plasma water with Ar gas using a DBD plasma jet reactor obtained a similar pH compared to our result (pH ranging from 6 to 8) [2]. The PAW-O_2 obtained a higher pH value than the PAW-N_2 and the PAW-air. This is similarly due to the lack of nitrogen which results in lower concentrations of NO_3^- and NO_2^- ions in the PAW [41]. Notably, there is no significant difference in the temperature among four types of PAWs used in this study, ranging from 41.27 ± 0.15℃ to 44.50 ± 0.36℃ (Fig. 3B). Other studies also found that the effect of temperature can be insignificant on the antimicrobial activity against bacteria biofilms [19].

To further characterise the PAW activity, the electrical conductivity (EC) of the PAW generated using different gases was determined. EC is a measure of how easily an electrical charge can pass through a material or liquid (e.g., water). A higher EC may be related to enhanced antimicrobial activity [43]. We have observed a significantly ($p < 0.05$) higher EC of the PAW when air (240.30 ± 31.98 µS•cm^{-1}) and N_2 (125.10 ± 12.34 µS•cm^{-1}) were used as the plasma-forming gas. This can be attributed to a larger amount of NO_x (resulting in a lower pH) present in the plasma phase in comparison to the PAW-Ar (20.96 ± 8.65 µS•cm^{-1}) and the PAW-O_2 (14.20 ± 6.69 µS•cm^{-1}). A similar result where the conductivity of MilliQ water increases after the plasma

treatment was reported elsewhere [41]. The EC follows a similar trend to NO_x (Fig. 3A) which supports the reliability of the results since the EC and NO_x are strongly interdependent with each other.

Another indicator for antibacterial activity is ORP as it provides a measure of how oxidizing the PAW is and thus shows its potential to inactivate microorganisms. Our data show an increase in ORP for all four PAW types compared to the MilliQ control (Fig. 3D). The highest ORP was measured for the PAW-O_2. This correlates with the highest CFU reduction of the PAW-O_2 compared to the other gases. Several studies have demonstrated an ORP increase with increasing the PAW generation time and that was correlated with a higher antimicrobial activity [16,17, 39].

3.3. Optical emission spectra of PAW discharge

The representative emission spectrum and the identified emission bands of the bubble discharge plasma ranging from 200 to 900 nm of wavelength was shown in Fig. 4. The OES spectra of air and nitrogen BSDs (Fig. 4. A and B) exhibited predominantly excited nitrogen species, including the second positive system (SPS) of molecule nitrogen N_2 ($C^3\Pi_u \rightarrow B^3\Pi_g$) at 300–470 nm, the first negative system (FNS) of molecular nitrogen ion N_2^+ ($B^2\Sigma_u^+ \rightarrow X^2\Sigma_g^+$) at 391 and 427 nm, and the first positive system (FPS) of molecular nitrogen N_2 ($B^3\Pi_g \rightarrow A^3\Sigma^+$) ranging between 500 nm and 800 nm. The emission spectra of Ar discharge in Fig. 4(C) shows higher emission intensity from hydroxyl radicals (306.5 nm and 600–650 nm) and excited oxygen (777 nm and 844 nm) and hydrogen atoms (656 nm) as overall emission intensity significantly higher compared to the rest. A recent study [2] of dielectric discharge barrier plasma with argon, oxygen, nitrogen, and air gases interaction with distilled water presented similar optical emission spectra to air and nitrogen discharge (Fig. 4A and B) from this work, while their OH emission results do not agree with the emission of the energy state OH (A) to ground state OH(X) in Ar and O_2 BSDs observed in this work (Fig. 4C and D). The emission spectra of O_2 discharge (Fig. 4D) exhibited a lower radical density compared to that of Ar BSD, which might be due to low ionization, vibrational and electronic excitation as well as H_2O dissociation reaction of O_2 plasma compared to Ar plasma (see in supportive information Fig. S5). Moreover, from our V-I measurement (Fig. S4) and energy loss fraction calculation (see in supportive information Table. S1, and Fig. S5), Ar BSD generated the highest average power in comparison with air, N_2, and O_2 BSDs, which enables high-density excited OH(A) resulting in enhanced emission intensity of OH(A→X).

Based on the OES measurement results, we summarised the possible important gas phase reactions in PAW-N_2, PAW-air, PAW-Ar, and PAW-O_2 BSD plasmas interacting with water molecules within gas bubbles.

$$e + H_2O \rightarrow \bullet OH + H + e \quad (1)$$

$$e + H_2O \rightarrow H_2O^* + e \quad (2)$$

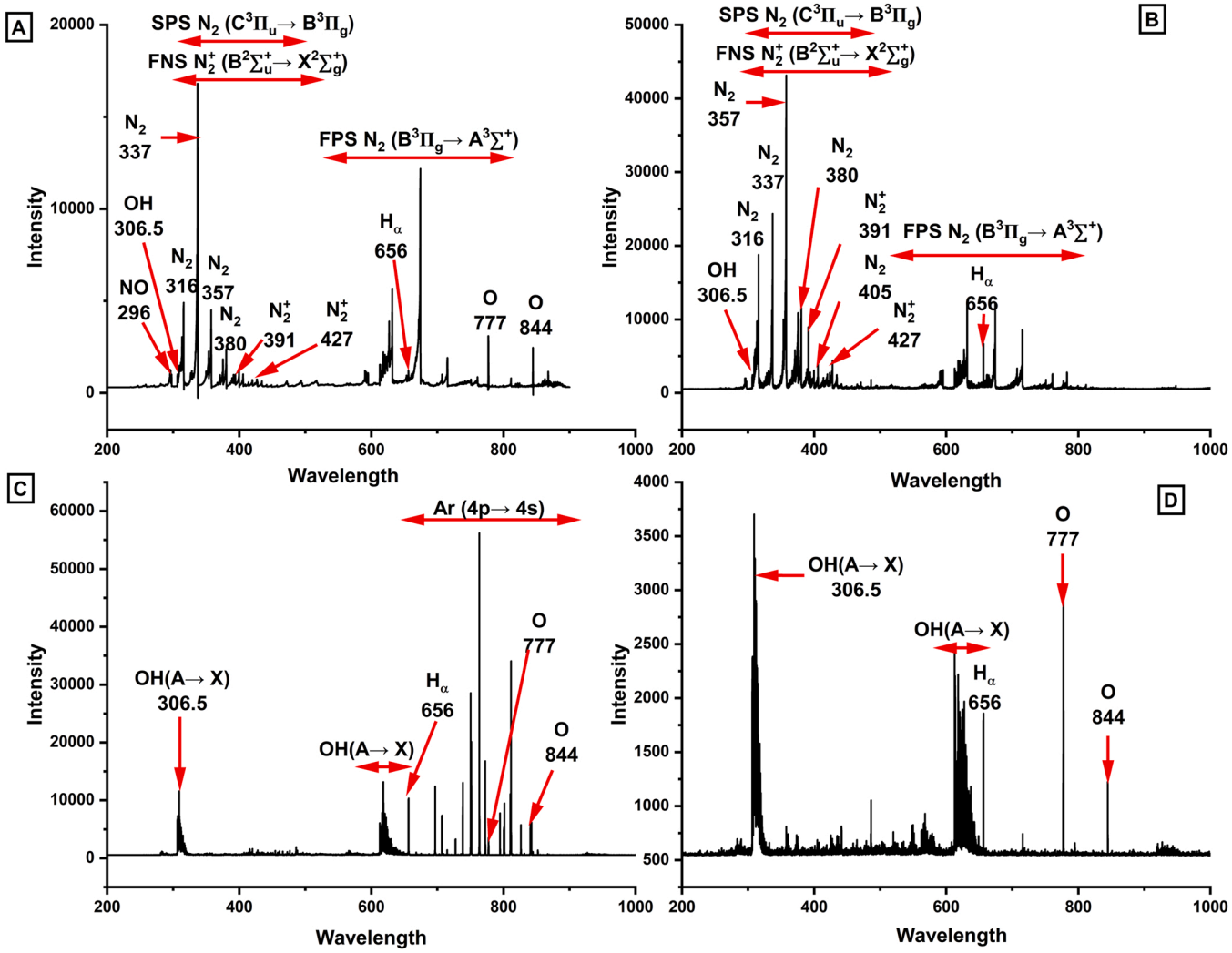

Fig. 4. Optical emission spectroscopy for A) air, B) nitrogen, C) argon, and D) oxygen bubble spark discharge plasma in interaction with MilliQ water.

$$e + H_2O^* \rightarrow H_2O^+ + 2e \quad (3)$$

$$H_2O + H_2O^+ \rightarrow \bullet OH + H_3O^+ \quad (4)$$

$$H_2O + h\nu \rightarrow \bullet OH + H \quad (5)$$

$$H_2O + M^* \rightarrow \bullet OH + H + M \quad (6)$$

The M* represents the excited neutral species, such as excited nitrogen, oxygen and argon species, in reaction 6.

In nitrogen BSD plasma, excited nitrogen atoms and molecules take important roles to sustain reactive plasma conditions as well as electron interactions such as dissociation and excitation.

$$N_2 + e \rightarrow N + N + e \quad (7)$$

$$N_2 + e \rightarrow N_2^* + e \quad (8)$$

$$N^* + H_2O \rightarrow N + \bullet OH + H \quad (9)$$

$$N^* + H_2O \rightarrow NH + \bullet OH \quad (10)$$

$$N_2^* + H_2O \rightarrow H + \bullet OH + N_2 \quad (11)$$

Regarding oxygen BSD plasma, various forms of reactive oxygen species can be generated including excited oxygen molecular and atomic species, ions and ozone, superoxide anion radicals and also hydrogen radicals through the interaction with water or its derivatives such as OH^- or HO_2 [2]:

$$O_2 + e \rightarrow O^+ + O + 2e \quad (12)$$

$$O_2 + e \rightarrow O^- + O \quad (13)$$

$$O + O_2 \rightarrow O_3 \quad (14)$$

$$O + H_2O \rightarrow 2OH\bullet \quad (15)$$

$$O_3 + OH^- \rightarrow HO_2^- + O_2 \quad (16)$$

$$O_3 + HO_2^- \rightarrow OH \bullet + O_2^- + O_2 \quad (17)$$

In the case of air BSD plasma, on top of the above-mentioned important reactions in N_2 and O_2 plasma, additional chemical reactions between nitrogen and oxygen species need to be addressed to explain NO_x generation [2,60].

$$N + O + M \rightarrow \bullet NO + \mathrm{M} \quad (18)$$

$$N + O_2 \rightarrow \bullet NO + O \quad (19)$$

$$O + N_2 \rightarrow \bullet NO + N \quad (20)$$

In Reaction (18), M indicates background molecules such as N_2 or O_2 species in air discharge as a third body to absorb released energy.

In the argon BSD plasma, the presence of high-density metastable Ar* species is demonstrated by the measured strong optical emission between 690 and 912 nm (Fig. 4C) from the transition Ar(4p) to Ar(4 s) states. As shown in the reaction (23), high energy Ar* (11.55 eV) metastables can induce further ionization which is fundamentally important characteristics of Ar discharge to sustain high-density plasma even at low applied voltage conditions. This metastable Ar* species contribute to effectively generating hydroxyl radicals by the interaction with water molecules[58].

$$Ar + e \rightarrow Ar^+ + e + e \quad (21)$$

$$Ar + e \rightarrow Ar^* + e \quad (22)$$

$$Ar^* + Ar^* \rightarrow Ar^* + Ar^+ + 2e \quad (23)$$

$$Ar^* + H_2O \rightarrow Ar + \bullet OH + H \quad (24)$$

Overall, the above OES measurement combined with the suggested mechanism from the literature supports the experimental observations on the generation of reactive species such as OH•, O_2^-, NO•, and excited atoms in the gas phase of BSDs plasma, which then leads to the solvation and diffusion of RONS at the bubble-water interface and formation of activated water.

3.4. The use of molecular scavengers to detect reactive species in PAW

Measuring H_2O_2, NO_3^-, NO_2^- and other physical characteristics of the PAW helps shed some light on the antibacterial effects of the generated PAW. However, these measurements do not fully explain why the PAW-O_2 has the highest CFU reduction. We, therefore, used several molecular scavengers, including mannitol (scavenges OH•), uric acid (UA, scavenges O_3), Tiron (scavenges O_2^-), N-Acetyl-L-cysteine (NAC, scavenges ROS), and sodium pyruvate (SP, H_2O_2) to selectively remove reactive species from the PAW-O_2, and observed its effect on reducing for *E. coli* biofilms viability (Fig. 5). If removing a reactive species from the PAW-O_2 caused it to lose its antibacterial effect, it can be concluded that the scavenged specie(s) was responsible for the observed effect. The addition of the scavengers UA (O_3) and mannitol (OH) did not affect the CFU numbers, with no viable cells detected after their addition (Fig. 5). NAC (ROS) and SP (H_2O_2) prevented the complete removal of biofilm cells exposed to the PAW-O_2 with a few viable cells detected after the addition of those scavengers, however, this was not statistically significant compared to PAW-O_2 without scavengers. Only Tiron, the scavenger for the O_2^- radicals, was able to significantly prevent biofilm killing from exposure to the PAW-O_2 [45,52] (Fig. 5).

According to our findings (Fig. 5), the elimination of biofilm might be attributed to the presence of O_2^- radical and H_2O_2 within the ROS. A previous study has indicated that CAP-generated O_2^- radical and H_2O_2 can cause a considerable amount of tumour cell death, although their toxicity towards tumour cells was found to be inadequate when used

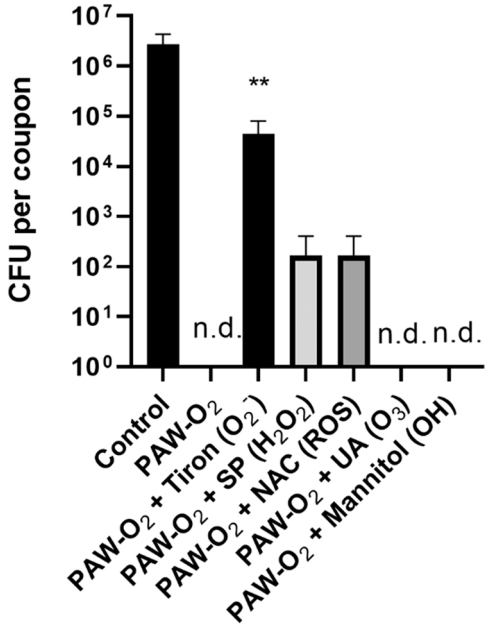

Fig. 5. CFU reduction of *E. coli* biofilms using PAW generated in oxygen with the addition of scavengers. 48 h biofilms were grown on stainless steel coupons and treated with PAW generated in oxygen in a bubble reactor. Scavengers (Tiron, NAC, SP, UA and Mannitol) were added directly to the PAW during generation. CFU reduction for PAW-O_2 with the superoxide anion scavenger Tiron is significantly different from the PAW-O_2 treatment without scavenger ($P < 0.01$, unpaired t-Test).

alone [61]. Moreover, the O_2^- radical is highly active and has been previously shown to substantially enhance the bactericidal effects of the PAW [31,45]. The oxygen toxicity of $\bullet O_2^-$ radicals is thought to be responsible for their antibacterial activity[59]. Though whether the detrimental effect of $\bullet O_2^-$ on the bacteria biofilm could be the inactivation of the bacterial dehydratases, an iron/sulphur clusters of proteins that are responsible for synthesizing branched-chain amino acids [22], its interaction with bacteria biofilm is still actively debated [59].

3.4.1. Detection of superoxide anion radicals in PAW

The fact that the addition of the superoxide scavenger Tiron to the PAW-O_2 was able to prevent biofilm removal suggests that superoxide is a major factor in the antibacterial activity of the PAW-O_2. We, therefore, aimed to detect $\bullet O_2^-$ in the PAW-O_2 using electron paramagnetic resonance (EPR) spectroscopy.

EPR combined with spin trap reagents (e.g. DMPO) has been broadly used in the detection of short-lived $\bullet O_2^-$ radicals [21]. However, the DMPO also reacts with •OH forming a relatively poor stable spin adducts DMPO-OH [67]. Thus, the resulting signal may also be attributed to •OH radicals. To overcome this and selectively detect $\bullet O_2^-$ species, the Tiron scavenger was used as a negative control to capture the potential $\bullet O_2^-$ in the PAW. Our EPR spectra results indicate that the DMPO had no hyperfine interaction with the non-plasma control (O_2 bubbling water) with only a small one-peak signal (Fig. 6A), while the DMPO showed four strong peaks with the ratio of 1:1:1:1 in the PAW-O_2 (Fig. 6B). These peaks are strongly associated with $\bullet O_2^-$ because these species were not observed when Tiron was added to the PAW-O_2 and thus no $\bullet O_2^-$ species was present (negative control) (Fig. 6C).

3.5. E. coli biofilm imaging characterisation

To investigate the effect of in situ PAW treatment on *E. coli* biofilms, cells were stained with live/dead kit after the treatment and observed under a confocal microscope (Fig. 7 A). The untreated control *E. coli* biofilms consisted of mainly live (green) cells with only a few dead cells (red) present. This was similar for the PAW- N_2 and the PAW-Ar (Fig. 7B and C) samples. In contrast, a significant number of dead cells occurred in biofilms treated with the PAW-air (Fig. 7D). While there were not many cells left on the PAW-O_2 treated biofilms, most of the cells were dead and approximately 91.4% of reduction in biofilm thickness compared to the control (Fig. 7 A and E). When Tiron (O_2^- scavenger) is added to the PAW-O_2 sample leading to a loss of efficacy of suspected

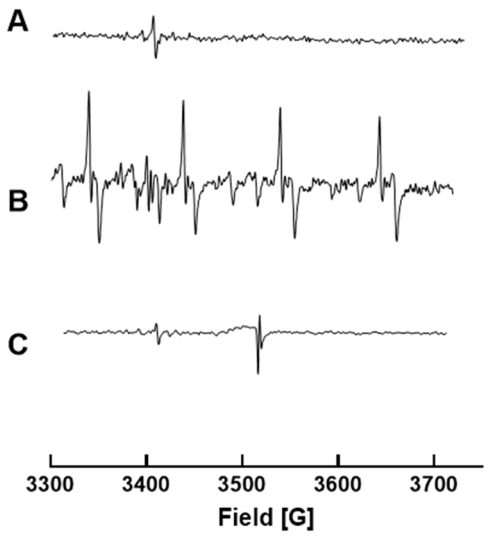

Fig. 6. Electron paramagnetic resonance spectra of 800 mM of DMPO with A) 60 s O_2 bubbling MQ water; B) 60 s PAW-O_2 treated MQ water; C) 60 s PAW-O_2 treated MQ water with 20 mM Tiron.

superoxide species, more viable biofilm cells can be observed (Fig. 7 F), which confirms the results of the scavengers' assay (Fig. 5). O_2^- radicals were apparently only able to form in the plasma generated using pure oxygen and not in other mixtures of O_2 and N_2 gases [55]. These fluorescent staining results, along with the results of the cell enumeration where the PAW-O_2 had the lowest CFU numbers n (Fig. 2), correlate with the activity of O_2^- radicals. It appears that direct PAW treatment can remove biofilms from the coupon, and cells that are still present are killed through inducing cell membrane damage. This has been previously observed for a *Listeria monocytogenes* biofilm model [5,20], after 15 min plasma water treatments, with the inactivation occurring in the biofilm centre and expanding to the edges. That study also showed that the treated biofilm matrix appeared as a homogenous structure with a 60% reduction in thickness compared to the control (10 μm).

3.6. Intracellular detection of RONS in E. coli biofilms

To investigate the role of oxidative stress induced by the PAW-O_2, fluorescence staining with DCFDA was used to detect the accumulated ROS in *E. coli* biofilm. DCFDA is a cell-permeable and upon oxidation (e.g., via RONS created in the PAW) is converted to the fluorescent dichlorofluorescein (DCF) that can be measured in a plate reader. After treatment with the PAW-O_2 (Fig. 8), ROS levels were increased significantly by approximately 4.5-fold compared to the control. While the addition of 20 mM of Tiron (O_2^- scavenger) to the PAW-O_2 treated biofilms resulted in significantly less accumulation of ROS (Fig. 8). These data suggest that O_2^- radicals play an important role in intracellular ROS accumulation and may be responsible for the significant biofilms removal caused by PAW-O_2. However, the mechanism of O_2^- radicals penetrating the biofilm matrix is still unclear. One study found that the O_2^- radicals could penetrate and attack the targeted bacteria membrane under an acidic environment [25]. This might lead to the accumulation of ROS within the biofilm cells.

In this study, the PAW generated with O_2 showed the greatest antibacterial activity against 48 h *E. coli* biofilms, demonstrating a 6-log reduction, compared to biofilms treated with PAW generated with inputs of air, N_2, and Argon. The confocal microscopy images also revealed the removal of biofilms from the coupon surface with only dead cells remaining after the PAW-O_2 treatment. An acidic pH, a higher ORP, and the presence of H_2O_2, NO_3^-, and NO_2^- generated in the PAW were widely studied as the mechanisms behind the antibacterial activities of the PAW [54]. However, the presence of superoxide anion radical appears to play a major role in PAW-mediated biofilm removal. While H_2O_2, NO_2^-, and NO_3^- were detected by quantitative tests and they are strong oxidants, their impacts were limited in our system because their concentrations are less than the effective biofilm killing concentration of 1000 mg/L of HNO_3 and H_2O_2 in this study (see supportive information Fig. S2). We also confirm that the elevated levels of intracellular ROS in *E. coli* biofilms after PAW-O_2 treatment suggesting that superoxide anion radical plays a crucial role in inducing a high intracellular oxidative stress within *E. coli* biofilms cells in response to the PAW-O_2 treatment.

4. Conclusions

In summary, a bubble spark discharge (BSD) with an input gas of oxygen generated plasma-activated water (PAW) can completely remove 48 h *E. coli* biofilms grown on stainless-steel surfaces. The short-lived superoxide anion radical was found to be a decisive factor in the antimicrobial effect caused by direct exposure to PAW-O_2. Input gas sources of atmospheric air, argon, and nitrogen were used to generate PAW, and were found to generate a mixture of reactive species with variable biofilm removal efficacy.

This research presents new knowledge on the use of PAW to remove bacterial biofilms and points to the importance of short-lived reactive species in the observed antibacterial efficacy. This has implications for drinking and wastewater water treatment, as well as possible treatment

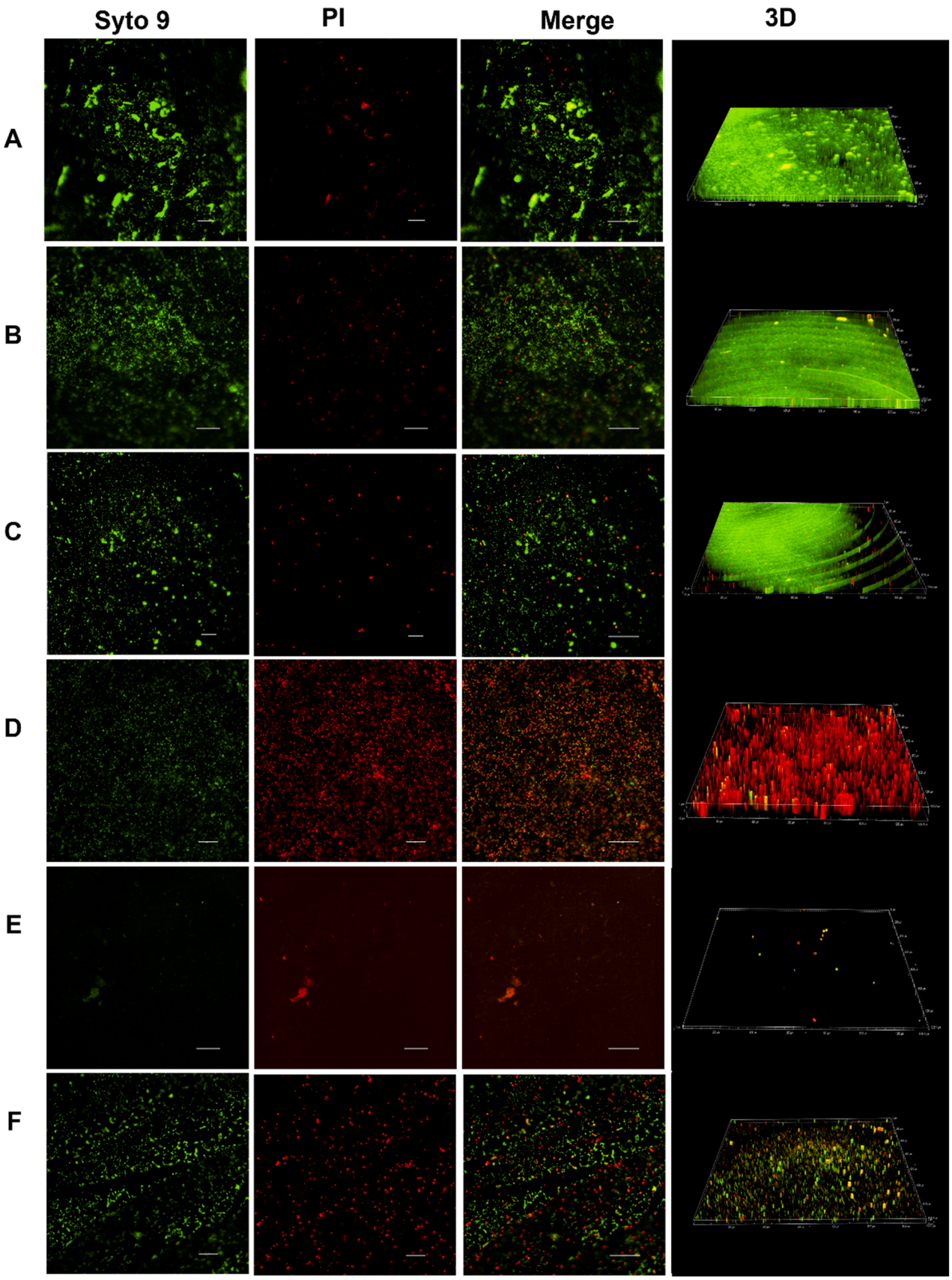

Fig. 7. PAW-induced *E. coli* biofilm removal. Biofilms were stained using live/dead kit and observed with an inverted Nikon Ti-E confocal microscope. 3D Z-stack images (upper and lower side of coupon surfaces) are presented on the right column. All images were taken with a x40 magnification. The scale bar is 50 μm. A) control, B) PAW-N_2, C) PAW-Ar, D) PAW-air, E) PAW-O_2 and F) PAW-O_2 + Tiron scavenger. Experiments were repeated three times and a minimum of five images were taken for each observed stainless-steel coupon.

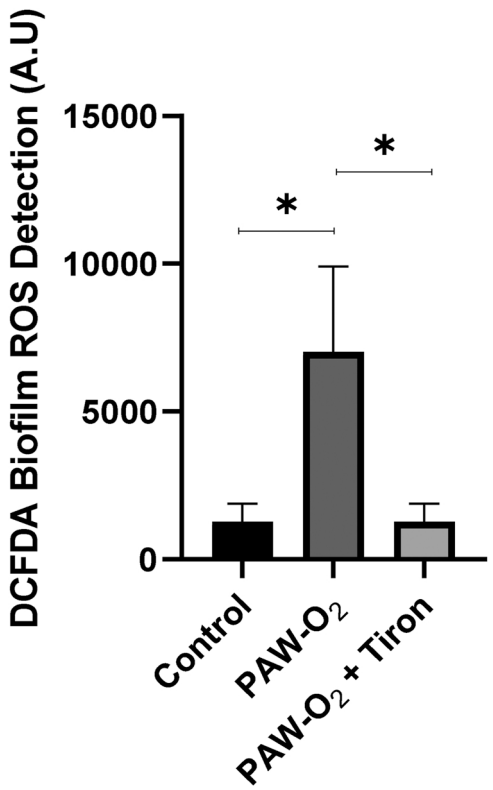

Fig. 8. Detection of intracellular ROS in *E. coli* biofilms following treatment with PAW-O_2, PAW-O_2 + Tiron, and Control. ROS was measured using DCFDA staining of the 48 h biofilms. The presence of ROS is significantly higher in biofilms treated with the PAW-O_2 compared to biofilms treated with the PAW-O_2 + Tiron and control (MilliQ) ($P < 0.05$, One-Way ANOVA with Tukey's multiple comparisons test).

of food products or medical devices where conventional disinfection or sanitation is neither suitable, nor effective. Utilising compressed atmospheric air (or oxygen) as a gas input source is an economically viable option when generating PAW. This further underscores its attractiveness for use. Lastly, the plasma source used in this work also has the advantage of being small and portable making it suitable for diverse applications in the water treatment industry, food industry, clinical equipment sterilization, medicine, and environment.

CRediT authorship contribution statement

Binbin Xia: Conceptualization, Methodology, Investigation, Validation, Data curation, Formal analysis, Writing – original draft. **Heema Kumari Nilesh Vyas**: Investigation, Methodology, Writing – review & editing. **Renwu Zhou**: Investigation, Formal data analysis, Writing – review & editing. **Tianqi Zhang**: Resources. **Jungmi Hong**: Investigation, Data curation, Formal data analysis, Writing – review & editing. **Joanna G. Rothwell**: Writing – review & editing. **Scott A. Rice**: Writing – review & editing, Project administration, Funding acquisition. **Dee Carter:** Writing – review & editing, Project administration, Funding acquisition. **Kostya (Ken) Ostrikov**: Writing – review & editing. **Patrick J. Cullen**: Supervision. **Anne Mai-Prochnow**: Conceptualization, Supervision, Investigation, Formal data analysis, Writing – review & editing, Funding acquisition, Project administration.

Declaration of Competing Interest

The authors declare the following financial interests/personal relationships which may be considered as potential competing interests: Author PJ Cullen is the CEO of PlasmaLeap Technologies, the supplier of the plasma power source and reactors employed in this study.

Data Availability

Data will be made available on request.

Acknowledgements

Funding: This work was supported by the Australian Research Council [grant number DP210101358].

Appendix A. Supporting information

Supplementary data associated with this article can be found in the online version at doi:10.1016/j.jece.2023.109977.

References

[1] G.G. Bălan, I. Roşca, E.-L. Ursu, F. Doroftei, A.-C. Bostănaru, E. Hnatiuc, V. Năstasă, V. Şandru, G. Ştefănescu, A. Trifan, Plasma-activated water: a new and effective alternative for duodenoscope reprocessing, Infect. Drug Resist. 11 (2018) 727.
[2] N. Bolouki, W.-H. Kuan, Y.-Y. Huang, J.-H. Hsieh, Characterizations of a plasma-water system generated by repetitive microsecond pulsed discharge with air, Nitrogen, Oxyg., Argon. Gases Species Appl. Sci. 11 (13) (2021) 6158.
[3] M. Cámara, W. Green, C.E. MacPhee, P.D. Rakowska, R. Raval, M.C. Richardson, J. Slater-Jefferies, K. Steventon, J.S. Webb, Economic significance of biofilms: a multidisciplinary and cross-sectoral challenge, npj Biofilms Micro 8 (1) (2022) 42.
[4] P. Chakraborty, S. Bajeli, D. Kaushal, B.D. Radotra, A. Kumar, Biofilm formation in the lung contributes to virulence and drug tolerance of *Mycobacterium tuberculosis*, Nat. Commun. 12 (2021) 1.
[5] T.-P. Chen, J. Liang, T.-L. Su, Plasma-activated water: antibacterial activity and artifacts? Environ. Sci. Pollut. Res. 25 (27) (2018) 26699–26706.
[6] J.W. Costerton, P.S. Stewart, E.P. Greenberg, Bacterial biofilms: a common cause of persistent infections, Sci. (N. Y., N. Y.) 284 (5418) (1999) 1318–1322.
[7] P.J. Cullen, J. Lalor, L. Scally, D. Boehm, V. Milosavljević, P. Bourke, K. Keener, Translation of plasma technology from the lab to the food industry, Plasma Process. Polym. 15 (2) (2018) 1700085.
[8] S. Dula, T.A. Ajayeoba, O.A. Ijabadeniyi, Bacterial biofilm formation on stainless steel in the food processing environment and its health implications, Folia Microbiol. 66 (3) (2021) 293–302.
[9] P. Fernández-Gómez, J.F. Cobo-Díaz, M. Oliveira, M. González-Raurich, A. Alvarez-Ordóñez, M. Prieto, J.L. Walsh, M. Sivertsvik, E. Noriega-Fernández, M. López, Susceptibility and transcriptomic response to plasma-activated water of Listeria monocytogenes planktonic and sessile cells, Food Microbiol 113 (2023), 104252.
[10] P.B. Flynn, W.G. Graham, B.F. Gilmore, Acinetobacter baumannii biofilm biomass mediates tolerance to cold plasma, Lett. Appl. Microbiol. 68 (4) (2019) 344–349.
[11] Y. Gao, M. Li, C. Sun, X. Zhang, Microbubble-enhanced water activation by cold plasma, Chem. Eng. J. 446 (2022), 137318.
[12] B. Ghimire, E.J. Szili, B.L. Patenall, P. Lamichhane, N. Gaur, A.J. Robson, D. Trivedi, N.T. Thet, A.T.A. Jenkins, E.H. Choi, R.D. Short, Enhancement of hydrogen peroxide production from an atmospheric pressure argon plasma jet and implications to the antibacterial activity of plasma activated water, Plasma Sources Sci. Technol. 30 (3) (2021), 035009.
[13] B.F. Gilmore, P.B. Flynn, S. O'Brien, N. Hickok, T. Freeman, P. Bourke, Cold plasmas for biofilm control: opportunities and challenges, Trends Biotechnol. 36 (6) (2018) 627–638.
[14] F. Girard, M. Peret, N. Dumont, V. Badets, S. Blanc, K. Gazeli, C. Noël, T. Belmonte, L. Marlin, J.-P. Cambus, G. Simon, N. Sojic, B. Held, S. Arbault, F. Clément, Correlations between gaseous and liquid phase chemistries induced by cold atmospheric plasmas in a physiological buffer, Phys. Chem. Chem. Phys. 20 (14) (2018) 9198–9210.
[15] D. Guo, H. Liu, L. Zhou, J. Xie, C. He, Plasma-activated water production and its application in agriculture, J. Sci. Food Agric. 101 (12) (2021) 4891–4899.
[16] J. Guo, K. Huang, X. Wang, C. Lyu, N. Yang, Y. Li, J. Wang, Inactivation of Yeast on Grapes by Plasma-Activated Water and Its Effects on Quality Attributes, J. Food Prot. 80 (2) (2017) 225–230.
[17] J. Guo, D. Qin, W. Li, F. Wu, L. Li, X. Liu, Inactivation of *Penicillium italicum* on kumquat via plasma-activated water and its effects on quality attributes, Int. J. Food Microbiol. (2021) 343.
[18] G. Haghighat, A. Sohrabi, P.M. Shaibani, C.W. Van Neste, S. Naicker, T. Thundat, The role of chloride ions in plasma-activated water treatment processes, Environ. Sci.: Water Res. Technol. 3 (1) (2017) 156–168.
[19] O. Handorf, H. Below, U. Schnabel, K. Riedel, J. Ehlbeck, Investigation of the chemical composition of plasma-treated water by MidiPLexc and its antimicrobial effect on L. monocytogenes and Pseudomonas fluorescens monospecies suspension cultures, J. Phys. D: Appl. Phys. 53 (30) (2020), 305204.
[20] O. Handorf, V.I. Pauker, T. Weihe, J. Schäfer, E. Freund, U. Schnabel, S. Bekeschus, K. Riedel, J. Ehlbeck, Plasma-Treated Water Affects Listeria monocytogenes Vitality and Biofilm Structure, Front. Microbiol. 12 (2021), 652481.

[21] X. Hu, Y. Zhang, R.A. Wu, X. Liao, D. Liu, P.J. Cullen, R.-W. Zhou, T. Ding, Diagnostic analysis of reactive species in plasma-activated water (PAW): current advances and outlooks, J. Phys. D: Appl. Phys. 55 (2) (2021), 023002.
[22] J.A. Imlay, Pathways of oxidative damage, Annu. Rev. Microbiol. 57 (1) (2003) 395–418.
[23] K. Jenns, H.P. Sassi, R. Zhou, P.J. Cullen, D. Carter, A. Mai-Prochnow, Inactivation of foodborne viruses: Opportunities for cold atmospheric plasma, Trends Food Sci. Technol. (2022).
[24] N.K. Kaushik, B. Ghimire, Y. Li, M. Adhikari, M. Veerana, N. Kaushik, N. Jha, B. Adhikari, S.J. Lee, K. Masur, T. von Woedtke, K.D. Weltmann, E.H. Choi, Biological and medical applications of plasma-activated media, water and solutions, Biol. Chem. 400 (1) (2018) 39–62.
[25] S.S. Korshunov, J.A. Imlay, A potential role for periplasmic superoxide dismutase in blocking the penetration of external superoxide into the cytosol of Gram-negative bacteria, Mol. Microbiol. 43 (1) (2002) 95–106.
[26] W. Li, R. Zhou, R. Zhou, J. Weerasinghe, T. Zhang, A. Gissibl, P.J. Cullen, R. Speight, K. Ostrikov, Insights into amoxicillin degradation in water by non-thermal plasmas, Chemosphere 291 (2022), 132757.
[27] W. Li, R. Zhou, R. Zhou, J. Weerasinghe, T. Zhang, A. Gissibl, P.J. Cullen, R. Speight, K.K. Ostrikov, Insights into amoxicillin degradation in water by non-thermal plasmas, Chemosphere 291 (2022), 132757.
[28] Y. Li, J. Pan, G. Ye, Q. Zhang, J. Wang, J. Zhang, J. Fang, In vitro studies of the antimicrobial effect of non-thermal plasma-activated water as a novel mouthwash, Eur. J. Oral. Sci. 125 (6) (2017) 463–470.
[29] L. Lin, H. Quoc Pho, L. Zong, S. Li, N. Pourali, E. Rebrov, N. Nghiep Tran, K. Ostrikov, V. Hessel, Microfluidic plasmas: Novel technique for chemistry and chemical engineering, Chem. Eng. J. 417 (2021), 129355.
[30] P. Lu, C. Chen, Q. Wang, Z. Wang, X. Zhang, S. Xie, Phylogenetic diversity of microbial communities in real drinking water distribution systems, Biotechnol. Bioprocess Eng. 18 (1) (2013) 119–124.
[31] M. Ma, Y. Zhang, Y. Lv, F. Sun, The key reactive species in the bactericidal process of plasma activated water, J. Phys. D: Appl. Phys. 53 (18) (2020), 185207.
[32] R. Ma, G. Wang, Y. Tian, K. Wang, J. Zhang, J. Fang, Non-thermal plasma-activated water inactivation of food-borne pathogen on fresh produce, J. Hazard. Mater. 300 (2015) 643–651.
[33] A. Mai-Prochnow, D. Alam, R. Zhou, T. Zhang, K. Ostrikov, P.J. Cullen, Microbial decontamination of chicken using atmospheric plasma bubbles, Plasma Process Polym. N./a(N./a) (2020), e2000052.
[34] A. Mai-Prochnow, M. Bradbury, K. Ostrikov, A.B. Murphy, Pseudomonas aeruginosa biofilm response and resistance to cold atmospheric pressure plasma is linked to the redox-active molecule phenazine, PLOS ONE 10 (6) (2015), e0130373.
[35] A. Mai-Prochnow, M. Clauson, J. Hong, A.B. Murphy, Gram positive and Gram negative bacteria differ in their sensitivity to cold plasma, Sci. Rep. 6 (1) (2016) 38610.
[36] A. Mai-Prochnow, R. Zhou, T. Zhang, K.K. Ostrikov, S. Mugunthan, S.A. Rice, P. J. Cullen, Interactions of plasma-activated water with biofilms: inactivation, dispersal effects and mechanisms of action, npj Biofilms Micro 7 (1) (2021) 1–12.
[37] C. Man, C. Zhang, H. Fang, R. Zhou, B. Huang, Y. Xu, X. Zhang, T. Shao, Nanosecond-pulsed microbubble plasma reactor for plasma-activated water generation and bacterial inactivation, Plasma Process. Polym. 19 (6) (2022) 2200004.
[38] A.I. Muhammad, X. Liao, P.J. Cullen, D. Liu, Q. Xiang, J. Wang, S. Chen, X. Ye, T. Ding, Effects of nonthermal plasma technology on functional food components, Compr. Rev. Food Sci. Food Saf. 17 (5) (2018) 1379–1394.
[39] J. Pan, Y.L. Li, C.M. Liu, Y. Tian, S. Yu, K.L. Wang, J. Zhang, J. Fang, Investigation of cold atmospheric plasma-activated water for the dental Unit waterline system contamination and safety evaluation in vitro, Plasma Chem. Plasma Process. 37 (4) (2017) 1091–1103.
[40] V. Rathore, S.K. Nema, Optimization of process parameters to generate plasma activated water and study of physicochemical properties of plasma activated solutions at optimum condition, J. Appl. Phys. 129 (2021) 8.
[41] V. Rathore, D. Patel, S. Butani, S.K. Nema, Investigation of physicochemical properties of plasma activated water and its bactericidal efficacy, Plasma Chem. Plasma Process. 41 (3) (2021) 871–902.
[42] V. Rathore, D. Patel, S. Butani, S.K. Nema, Investigation of physicochemical properties of plasma activated water and its bactericidal efficacy, Plasma Chem. Plasma P (2021).
[43] M. Rehan, A.A. Nada, T.A. Khattab, N.A.M. Abdelwahed, A.A.A. El-Kheir, Development of multifunctional polyacrylonitrile/silver nanocomposite films: antimicrobial activity, catalytic activity, electrical conductivity, UV protection and SERS-active sensor, J. Mater. Res. Technol. 9 (4) (2020) 9380–9394.
[44] T.-Y. Renn, C.-P. Yang, U.-I. Wu, L.-Y. Chen, F.-D. Mai, M.A. Tikhonova, T. G. Amstislavskaya, W.-C. Liao, C.-T. Lin, Y.-C. Liu, H.-M. Chang, Water composed of reduced hydrogen bonds activated by localized surface plasmon resonance effectively enhances anti-viral and anti-oxidative activities of melatonin, Chem. Eng. J. 427 (2022), 131626.
[45] J.G. Rothwell, D. Alam, D.A. Carter, B. Soltani, R. McConchie, R. Zhou, P.J. Cullen, A. Mai-Prochnow, The antimicrobial efficacy of plasma-activated water against Listeria and E. coli is modulated by reactor design and water composition, J. Appl. Microbiol. 132 (4) (2022) 2490–2500.
[46] T. Royintarat, P. Seesuriyachan, D. Boonyawan, E.H. Choi, W. Wattanutchariya, Mechanism and optimization of non-thermal plasma-activated water for bacterial inactivation by underwater plasma jet and delivery of reactive species underwater by cylindrical DBD plasma, Curr. Appl. Phys. 19 (9) (2019) 1006–1014.
[47] Y. Sen, M. Mutlu, Sterilization of food contacting surfaces via non-thermal plasma treatment: a model study with escherichia coli-contaminated stainless steel and polyethylene surfaces, Food Bioprocess Tech. 6 (12) (2013) 3295–3304.
[48] K.F. Sergeichev, N.A. Lukina, R.M. Sarimov, I.G. Smirnov, A.V. Simakin, A. S. Dorokhov, S.V. Gudkov, Physicochemical properties of pure water treated by pure argon plasma jet generated by microwave discharge in opened atmosphere, Front. Phys. 8 (2021), 614684.
[49] J. Shen, Y. Tian, Y. Li, R. Ma, Q. Zhang, J. Zhang, J. Fang, Bactericidal effects against *S. aureus* and physicochemical properties of plasma activated water stored at different temperatures, Sci. Rep. -Uk 6 (2016) 28505.
[50] A. Soni, J. Choi, G. Brightwell, Plasma-activated water (PAW) as a disinfection technology for bacterial inactivation with a focus on fruit and vegetables, Foods 10 (1) (2021) 166.
[51] K. Stapelmann, O. Kylián, B. Denis, F. Rossi, On the application of inductively coupled plasma discharges sustained in Ar/O2/N2 ternary mixture for sterilization and decontamination of medical instruments, J. Phys. D: Appl. Phys. 41 (19) (2008), 192005.
[52] F.A. Taiwo, Mechanism of tiron as scavenger of superoxide ions and free electrons, Spectroscopy 22 (6) (2008) 491–498.
[53] J. Tan, M.V. Karwe, Inactivation and removal of Enterobacter aerogenes biofilm in a model piping system using plasma-activated water (PAW), Innov. Food Sci. Emerg. Technol. 69 (2021), 102664.
[54] R. Thirumdas, A. Kothakota, U. Annapure, K. Siliveru, R. Blundell, R. Gatt, V. P. Valdramidis, Plasma activated water (PAW): Chemistry, physico-chemical properties, applications in food and agriculture, Trends Food Sci. Technol. 77 (2018) 21–31.
[55] H. Tresp, M.U. Hammer, J. Winter, K. Weltmann, S. Reuter, Quantitative detection of plasma-generated radicals in liquids by electron paramagnetic resonance spectroscopy, J. Phys. D: Appl. Phys. 46 (43) (2013), 435401.
[56] K. Wan, L. Guo, C. Ye, J. Zhu, M. Zhang, X. Yu, Accumulation of antibiotic resistance genes in full-scale drinking water biological activated carbon (BAC) filters during backwash cycles, Water Res. (2021) 190.
[57] S. Wang, Y. Liu, R. Zhou, F. Liu, Z. Fang, K.K. Ostrikov, P.J. Cullen, Microsecond pulse gas–liquid discharges in atmospheric nitrogen and oxygen: Discharge mode, stability, and plasma characteristics, Plasma Process. Polym. 18 (2) (2021) 2000135.
[58] S. Wang, D. Yang, F. Liu, W. Wang, Z. Fang, Spectroscopic study of bipolar nanosecond pulse gas-liquid discharge in atmospheric argon, Plasma Sci. Technol. 20 (7) (2018), 075404.
[59] C.C. Winterbourn, Biological chemistry of superoxide radicals, ChemTexts 6 (1) (2020) 7.
[60] D. Xiao, C. Cheng, J. Shen, Y. Lan, H. Xie, X. Shu, Y. Meng, J. Li, P.K. Chu, Characteristics of atmospheric-pressure non-thermal N2 and N2/O2 gas mixture plasma jet, J. Appl. Phys. 115 (3) (2014), 033303.
[61] D. Xu, D. Liu, B. Wang, C. Chen, Z. Chen, D. Li, Y. Yang, H. Chen, M.G. Kong, In Situ OH generation from O2− and H2O2 plays a critical role in plasma-induced cell death, PLOS ONE 10 (6) (2015), e0128205.
[62] H. Xu, C. Liu, Q. Huang, Enhance the inactivation of fungi by the sequential use of cold atmospheric plasma and plasma-activated water: synergistic effect and mechanism study, Chem. Eng. J. 452 (2023), 139596.
[63] Z. Xu, X. Zhou, W. Yang, Y. Zhang, Z. Ye, S. Hu, C. Ye, Y. Li, Y. Lan, J. Shen, In vitro antimicrobial effects and mechanism of air plasma-activated water on Staphylococcus aureus biofilm, Plasma Process. Polym. 17 (8) (2020) 1900270.
[64] A.G. Yahaya, T. Okuyama, J. Kristof, M.G. Blajan, K. Shimizu, Direct and indirect bactericidal effects of cold atmospheric-pressure microplasma and plasma jet, Molecules 26 (9) (2021) 2523.
[65] Y. Zhao, L. Shao, L. Jia, Z. Meng, Y. Liu, Y. Wang, B. Zou, R. Dai, X. Li, F. Jia, Subcellular inactivation mechanisms of Pseudomonas aeruginosa treated by cold atmospheric plasma and application on chicken breasts, Food Res. Int. 160 (2022), 111720.
[66] R. Zhou, T. Zhang, R. Zhou, S. Wang, D. Mei, A. Mai-Prochnow, J. Weerasinghe, Z. Fang, K.K. Ostrikov, P.J. Cullen, Sustainable plasma-catalytic bubbles for hydrogen peroxide synthesis, Green. Chem. 23 (8) (2021) 2977–2985.
[67] R. Zhou, R. Zhou, P. Wang, Y. Xian, A. Mai-Prochnow, X. Lu, P.J. Cullen, K. Ostrikov, K. Bazaka, Plasma-activated water: generation, origin of reactive species and biological applications, J. Phys. D: Appl. Phys. 53 (30) (2020), 303001.